JOHANNES KEPLER UNIVERSITY LINZ

Institute of Computational Mathematics

An H^1-Kaczmarz Reconstructor for Atmospheric Tomography

Markus Eslitzbichler
Department of Mathematical Sciences
Norwegian University of Science and Technology
7491 Trondheim, Norway

Clemens Pechstein
Institute of Computational Mathematics, Johannes Kepler University
Altenberger Str. 69, 4040 Linz, Austria

Ronny Ramlau
Institute of Industrial Mathematics, Johannes Kepler University
Altenberger Str. 69, 4040 Linz, Austria

NuMa-Report No. 2012-12 December 2012

Technical Reports before 1998:

1995

95-1	Hedwig Brandstetter *Was ist neu in Fortran 90?*	March 1995
95-2	G. Haase, B. Heise, M. Kuhn, U. Langer *Adaptive Domain Decomposition Methods for Finite and Boundary Element Equations.*	August 1995
95-3	Joachim Schöberl *An Automatic Mesh Generator Using Geometric Rules for Two and Three Space Dimensions.*	August 1995

1996

96-1	Ferdinand Kickinger *Automatic Mesh Generation for 3D Objects.*	February 1996
96-2	Mario Goppold, Gundolf Haase, Bodo Heise und Michael Kuhn *Preprocessing in BE/FE Domain Decomposition Methods.*	February 1996
96-3	Bodo Heise *A Mixed Variational Formulation for 3D Magnetostatics and its Finite Element Discretisation.*	February 1996
96-4	Bodo Heise und Michael Jung *Robust Parallel Newton-Multilevel Methods.*	February 1996
96-5	Ferdinand Kickinger *Algebraic Multigrid for Discrete Elliptic Second Order Problems.*	February 1996
96-6	Bodo Heise *A Mixed Variational Formulation for 3D Magnetostatics and its Finite Element Discretisation.*	May 1996
96-7	Michael Kuhn *Benchmarking for Boundary Element Methods.*	June 1996

1997

97-1	Bodo Heise, Michael Kuhn and Ulrich Langer *A Mixed Variational Formulation for 3D Magnetostatics in the Space $H(rot) \cap H(div)$*	February 1997
97-2	Joachim Schöberl *Robust Multigrid Preconditioning for Parameter Dependent Problems I: The Stokes-type Case.*	June 1997
97-3	Ferdinand Kickinger, Sergei V. Nepomnyaschikh, Ralf Pfau, Joachim Schöberl *Numerical Estimates of Inequalities in $H^{\frac{1}{2}}$.*	August 1997
97-4	Joachim Schöberl *Programmbeschreibung NAOMI 2D und Algebraic Multigrid.*	September 1997

From 1998 to 2008 technical reports were published by SFB013. Please see
`http://www.sfb013.uni-linz.ac.at/index.php?id=reports`
From 2004 on reports were also published by RICAM. Please see
`http://www.ricam.oeaw.ac.at/publications/list/`
For a complete list of NuMa reports see
`http://www.numa.uni-linz.ac.at/Publications/List/`

An H^1-Kaczmarz reconstructor for Atmospheric Tomography

Markus Eslitzbichler*, Clemens Pechstein†, and Ronny Ramlau‡

December 14, 2012

Abstract

Atmospheric tomography is a prerequisite step before wavefront perturbations can be corrected in Multi Conjucate Adaptive Optics (MCAO) systems. Recently, the use of a Landweber-Kaczmarz iteration has been proposed to solve the tomography problem. However, due to the geometric partitioning of the update steps in this method, discontinuities in the solution appear that are physically implausible. We investigate augmenting the Landweber-Kaczmarz iteration with a smoothing step based on solving an elliptic partial differential equation to alleviate these discontinuities.

Keywords: Atmospheric tomography, Kaczmarz iteration, Adaptive Optics, Multi Conjugate Adaptive Optics

2010 Mathematics Subject Classification: 65R32, 45Q05, 85-08, 78A55

1 Introduction

As light passes through the atmosphere, inhomogeneous temperature distributions distort its wavefront, which degrades image quality of ground based astronomical telescopes. To counter this effect, modern telescopes use *adaptive optics* systems, which employ one or more deformable mirrors to correct for phase perturbations in the wavefronts caused by the atmosphere turbulences. The shape of the deformable mirrors (DM) has to be computed from wavefront measurements obtained from either natural or artificial (laser) guide stars. For the reconstruction of the DM shapes, the specific hardware design of the wavefront sensors, the structure of the atmosphere and harsh computational limits have to be taken into account.

In the case of Multi Conjugate Adaptive Optics (MCAO), multiple wavefront sensors as well as multiple deformable mirrors are employed to achieve a high degree of wavefront correction over a wide field of view. The wavefront measurements from multiple directions are used to solve the atmospheric tomography problem, i.e., the reconstruction of turbulent layers above the telescope. Atmospheric tomography is a limited-angle tomography problem and therefore severely ill-posed. Furthermore, the reconstruction has to be done within strict time limits: depending on the specific application and usage scenario, usually below 1 ms, which is related to the timeframe within which the turbulences are expected to be "frozen". Both direct and iterative methods have been applied to solve the atmospheric tomography problem. Matrix-vector-multiplication based methods have been investigated in [15, 20]. However, with growing hardware capabilities (such as the number and resolution of wavefront sensors), the resulting

*Department of Mathematical Sciences, Norwegian University of Science and Technology, 7491 Trondheim, Norway, markuses@math.ntnu.no

†Institute of Computational Mathematics, Johannes Kepler University, Altenberger Str. 69, 4040 Linz, Austria, clemens.pechstein@numa.uni-linz.ac.at

‡Institute of Industrial Mathematics, Johannes Kepler University, Altenberger Str. 69, 4040 Linz, Austria, ronny.ramlau@jku.at

systems of equations become very large. Iterative methods such as preconditioned conjugate gradients have also been studied for use in atmospheric tomography (cf., e.g., [8, 7, 22]).

In this paper, we investigate an extension of a Landweber-Kaczmarz based atmospheric reconstruction method introduced in [16]. The Landweber-Kaczmarz method is an iterative method that operates only on sub-domains of the turbulent layers in every iteration, which makes it computationally very competitive. It is particularly well suited for high dimensional ill-posed problems (cf, e.g., [3]). Note that we will always assume that the wavefronts have already been reconstructed from wavefront sensor measurements, using, e.g., the CuRe (Cumulative reconstructor) [23, 18]. In the particular case of atmospheric tomography, the iterative update steps are executed on overlapping domains of annuli formed by telescope apertures being projected onto different atmospheric layers and into different directions, see Figure 3. In [16], the space L^2 is used to model the atmosphere. In this case, discontinuities are introduced into the iterates of the Kaczmarz algorithm that are not physically plausible. However, statistical models show that atmospheric turbulences have much higher smoothness than L^2. Thus, we choose the Sobolev space H^1 as the space of turbulences. Choosing a different function space affects in particular the adjoint of the atmospheric tomography operator, which leads to an additional smoothing effect in the reconstruction that will be analyzed in more detail in Sections 3 and 4.

It turns out that the H^1 algorithm differs from the original algorithm only by an additional smoothing step, thus, we refer to the H^1 algorithm as the *smoothed* Landweber-Kaczmarz method.

The remainder of the paper is structured as follows. In Section 2, we give a mathematical description of the atmospheric tomography problem and the corresponding Landweber-Kaczmarz method. In Section 3 we introduce the *smoothed* Landweber-Kaczmarz method. We further analyze in detail the regularity of the smoothed reconstruction. Finally, Section 4 investigates the performance of the smoothed Landweber-Kaczmarz method compared to the conventional L^2 method.

2 Landweber-Kaczmarz Iteration for Atmospheric Tomography

In this section we will first introduce the notation necessary to formulate the atmospheric tomography problem. In order to solve the problem, i.e., to reconstruct the turbulent layers from incoming wavefronts of several guide stars, G operator equations have to be solved. The Landweber-Kaczmarz algorithm, which is introduced in Section 2.2, is a natural choice for the solution of the inverse problem. Note that we will restrict our analysis to the case of *natural* guide stars only. Thus, additional effects from laser guide stars such as the cone effect or spot elongation have not been taken into account. Additionally, we will always assume that the wavefronts have already been reconstructed from the wave front sensor measurements. Please note that the section is mainly based on [16].

2.1 Notation and Problem Formulation

As in [16], the telescope aperture Ω_T is modeled as an annulus with inner and outer radii t_i and t_o, respectively:

$$\Omega_T := \{\boldsymbol{r} \in \mathbb{R}^2 : t_i \leq \|\boldsymbol{r}\| \leq t_o\},$$

Note that the following analysis might also be applied to other geometric shapes. The disk describing the telescope can be embedded into $\mathbb{R}^3$ by setting the height coordinate $z = 0$. In atmospheric tomography, we do not aim at the reconstruction of the full turbulence profile above the telescope, in particular as there is simply not enough data available to achieve a reasonable reconstruction. Instead, the turbulence is modeled by a finite number of thin layers

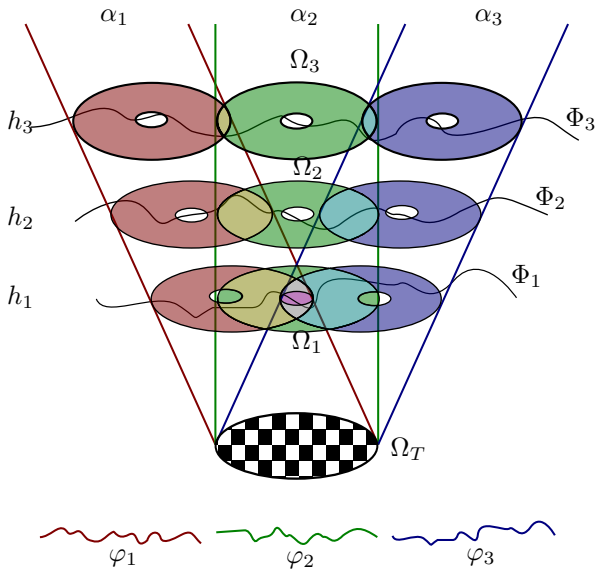

Figure 1: Notation for atmospheric tomography. The vectors $\boldsymbol{\alpha_g}$ denote the directions of guide stars. The functions Φ_ℓ represent turbulent atmospheric layers located at altitudes h_ℓ and defined on the domains Ω_ℓ. The incident wavefronts originating from the guide stars and measured by wavefront sensors are represented by the functions φ_g.

(cf., e.g., [17]). Each layer has to be understood as a two dimensional subset of a plane parallel to the telescope. Let L be the total number of the layers and let h_ℓ denote the altitude of the ℓ-th layer relative to the telescope, $\ell = 1, \dots, L$. Furthermore, let G be the number of guide stars and let $\boldsymbol{\alpha}_g \in \mathbb{R}^2$ denote the projection of the three-dimensional unit vector pointing from the centre $(0,0,0)$ of the telescope to guide star number g to the plane $\mathbb{R} \times \mathbb{R} \times \{0\}$, where $g = 1, \dots, G$. The area in layer ℓ covered by the g-th wavefront sensor is then given as

$$\Omega_{\ell,g} \;:=\; h_\ell \boldsymbol{\alpha}_g + \Omega_T \;=\; \{\boldsymbol{r} \in \mathbb{R}^2 : \boldsymbol{r} - h_\ell \boldsymbol{\alpha}_g \in \Omega_T\}.$$

Thus, the total area of layer ℓ covered by all wavefront sensors is simply given by

$$\Omega_\ell \;:=\; \bigcup_{g=1}^{G} \Omega_{\ell,g}\,,$$

i.e. the union of the shifted telescope apertures. For an illustration see Figure 1.
For each $\ell = 1, \dots, L$, let $V_\ell \subset L^2(\Omega_\ell)$ be the space of possible turbulences in layer ℓ. We assume that V_ℓ is a Hilbert space with inner product $\langle \cdot, \cdot \rangle_{V_\ell}$. Later on, V_ℓ will be chosen either as $L^2(\Omega_\ell)$ or $H^1(\Omega_\ell)$. By $\Phi_\ell \in V_\ell$ we denote the (unknown) turbulence in layer ℓ. As the turbulence in the atmosphere changes rapidly, Φ_ℓ generally depends on time. However, as we want to reconstruct the turbulence for a fixed time, the time dependency can be neglected. Furthermore, let $\varphi_g \in L^2(\Omega_T)$ denote the wavefront originating from guide star number g in direction $\boldsymbol{\alpha}_g$, $g = 1, \dots, G$ (see again Figure 1 for an illustration). Following [17], the wavefronts φ_g are related to the turbulent layers Φ_ℓ by

$$\varphi_g(\boldsymbol{r}) \;=\; \sum_{l=1}^{L} \Phi_\ell(\boldsymbol{r} + h_\ell \boldsymbol{\alpha}_g), \qquad \boldsymbol{r} \in \Omega_T,\, g = 1, \dots, G. \tag{1}$$

As we can see, the phase perturbations induced by the discrete layers are simply summed up along the line of sight. The sum $\varphi_g \in L^2(\Omega_T)$ is well-defined because $\Phi_\ell \in V_\ell \subset L^2(\Omega_\ell)$ and

the restriction of Φ_ℓ to $\Omega_{\ell,g}$ is again in L^2. In practice, the quantities φ_g are available via the reconstruction of the wavefront sensor measurements, whereas the turbulences Φ_ℓ are unknown and shall be be reconstructed from these data.

In order to devise a compact notation for Equation (1), we introduce the (linear) shift operators $T^{\boldsymbol{\alpha}_g,h_\ell} : L^2(\Omega_{\ell,g}) \to L^2(\Omega_T)$, given by

$$(T^{\boldsymbol{\alpha}_g,h_\ell}\theta)(\boldsymbol{r}) \;:=\; \theta(\boldsymbol{r} + h_\ell\boldsymbol{\alpha}_g) \qquad \text{for } \theta \in L^2(\Omega_{\ell,g}).$$

Moreover, let the product space $\boldsymbol{V} := \bigotimes_{\ell=1}^{L} V_\ell$ be equipped with the natural inner product

$$\langle \boldsymbol{\Phi},\, \boldsymbol{\Psi}\rangle_{\boldsymbol{V}} \;:=\; \sum_{\ell=1}^{L} \langle \Phi_\ell,\, \Psi_\ell\rangle_{V_\ell}\,. \tag{2}$$

Finally, we define the linear operator $\boldsymbol{P}_g : \boldsymbol{V} \to L^2(\Omega_T)$ by

$$\boldsymbol{P}_g\boldsymbol{\Phi} \;:=\; \sum_{\ell=1}^{L} T^{\boldsymbol{\alpha}_g,h_\ell}(\Phi_\ell|_{\Omega_{\ell,g}}), \tag{3}$$

which can be regarded as a *projection* operator. In vectorized form, the system of equations (1) now reads as

$$\boldsymbol{P}_g\boldsymbol{\Phi} = \varphi_g, \qquad g = 1,\dots,G, \tag{4}$$

where $\boldsymbol{\Phi} = (\Phi_1,\dots,\Phi_L)^T$ denotes the vector of unknown turbulences. Finally, we wish to remark that, in case of a 3 dimensional turbulence profile, the sum in (1) would turn into a line integral, which means we would have to solve a limited angle tomography problem from incomplete measurements (cf., e.g., [14]).

2.2 Solution with the Landweber-Kaczmarz Method

To solve system (4), we use a Landweber-Kaczmarz method (cf., e.g., [3, 11]), which reads in our context as follows: for a given initial guess $\boldsymbol{\Phi}^{(0)} \in \boldsymbol{V}$ for the turbulences, the iterates are given by

$$\boldsymbol{\Phi}^{(k+1)} \;:=\; \boldsymbol{\Phi}^{(k)} - \beta_k \boldsymbol{P}_g^*(\boldsymbol{P}_g\boldsymbol{\Phi}^{(k)} - \varphi_g), \qquad \text{with } g := 1 + (k \bmod G). \tag{5}$$

Above, β_k is a non-negative relaxation parameter and $\boldsymbol{P}_g^* : L^2(\Omega_T) \to \boldsymbol{V}$ denotes the adjoint of $\boldsymbol{P}_g$, given by the relation

$$\langle \boldsymbol{P}_g\boldsymbol{\Phi},\, \psi\rangle_{L^2(\Omega_T)} \;=\; \langle \boldsymbol{\Phi},\, \boldsymbol{P}_g^*\psi\rangle_{\boldsymbol{V}} \qquad \text{for } \boldsymbol{\Phi} \in \boldsymbol{V},\ \psi \in L^2(\Omega_T).$$

Obviously, each step of (5) operates only on a part of system (4). Specifically, for the definition (3) at hand, we make adjustments in the iterate only for one guidestar at a time.

As an important issue, let us note that the method inherently depends on the choice of the turbulence spaces $V_\ell \subset L^2(\Omega_\ell)$ and on their associated inner products, since different choices of spaces will lead to different adjoint operators $\boldsymbol{P}_g^*$. We will consider two cases:

(a) L^2-case: $V_\ell = L^2(\Omega_\ell)$, equipped with inner product

$$\langle v,\, w\rangle_{V_\ell} \;=\; \langle v,\, w\rangle_{L^2(\Omega_\ell)} \;:=\; \int_{\Omega_\ell} v\, w\, dx \tag{6}$$

and $\boldsymbol{A}_g : \bigotimes_{\ell=1}^{L} L^2(\Omega_\ell) \to L^2(\Omega_T)$ denote the corresponding projection operators $\boldsymbol{P}_g$ defined in (3). Then one can show that (see [16])

$$\boldsymbol{A}_g^*\psi \;=\; \big(\chi_{\Omega_{1,g}} \cdot (T^{\boldsymbol{\alpha}_g,h_1})^*\psi, \dots, \chi_{\Omega_{L,g}} \cdot (T^{\boldsymbol{\alpha}_g,h_L})^*\psi\big), \tag{7}$$

where $\chi_{\Omega_{\ell,g}}$ denote the characteristic functions. The adjoint $(T^{\boldsymbol{\alpha}_g,h_\ell})^* : L^2(\Omega_T) \to L^2(\Omega_{\ell,g})$ of the shift operator $T^{\boldsymbol{\alpha}_g,h_\ell}$ is simply given by the inverse shift, i.e.,

$$((T^{\boldsymbol{\alpha}_g,h_\ell})^*\psi)(\boldsymbol{r}) \;=\; \psi(\boldsymbol{r} - h_\ell\boldsymbol{\alpha}_g).$$

The Landweber-Kaczmarz algorithm for this case already delivers good results, both with respect to performance and quality of the solution (see [16]). However, due to the overlapping geometries $\Omega_{\ell,g}$ on which the update steps (5) are executed and due to the presence of the characteristic functions in (7), discontinuities in the solution arise, which are physically implausible.

(b) H^1-case: $V_\ell = H^1(\Omega_\ell)$, equipped with inner product

$$\langle v,\, w\rangle_{V_\ell} \;=\; \langle v,\, w\rangle_{H^1(\Omega_\ell)} \;:=\; \int_{\Omega_\ell} v\, w\, dx + \sigma \int_{\Omega_\ell} \nabla v \cdot \nabla w\, dx, \tag{8}$$

where σ is a positive parameter. In Section 3 below, we will give a motivation for this choice and comment on the role of the parameter σ.

Let $\boldsymbol{B}_g : \bigotimes_{\ell=1}^{L} H^1(\Omega_\ell) \to L^2(\Omega_T)$ denote the corresponding projection operators. If i_ℓ, $\ell = 1, \ldots, L$, denote the embedding operators from $H^1(\Omega_\ell)$ into $L^2(\Omega_\ell)$ and if

$$\mathbf{i} : \bigotimes_{\ell=1}^{L} H^1(\Omega_\ell) \to \bigotimes_{\ell=1}^{L} L^2(\Omega_\ell) \;:\; \boldsymbol{\Psi} \mapsto (\mathrm{i}_1\Psi_1,\, \ldots,\, \mathrm{i}_L\Psi_L) \tag{9}$$

denotes the corresponding embedding operator of the product spaces, it apparently follows that

$$\boldsymbol{B}_g \;=\; \boldsymbol{A}_g\mathbf{i} \qquad \text{and} \qquad \boldsymbol{B}_g^* \;=\; \mathbf{i}^*\boldsymbol{A}_g^*, \tag{10}$$

i.e., the adjoint projection operator $\boldsymbol{A}_g^*$ from the L^2-case is *augmented* by the adjoint $\mathbf{i}^*$. As we will see in the next section, the adjoint $\mathbf{i}^*$ has some smoothing effect. Therefore, when considering the H^1-case, we call the corresponding Landweber-Kaczmarz method a *smoothed Landweber-Kaczmarz* method.

Note that other smoothing approaches would be possible, but are not considered here.

3 Smoothed Landweber-Kaczmarz iteration

In this section, we study the smoothed Landweber-Kaczmarz method, which uses the adjoint $\mathbf{i}^*$ from the previous section for smoothing. In Section 3.1, we give a short motivation of the choice $V_\ell = H^1(\Omega_\ell)$ for the space of turbulences by considering the *von Karman turbulence model*, which is a statistical description of atmospheric turbulence. In Section 3.2, we show that the application of $\mathbf{i}^*$ corresponds to solving elliptic partial differential equations on the domains Ω_ℓ with a source function in L^2. In Section 3.3, the choice of the parameter σ is discussed. Finally, the smoothing effect of $\mathbf{i}^*$ is studied in Section 3.4.

3.1 Atmospheric Turbulences

Atmospheric turbulences are usually described using either the *Kolmogorov turbulence model* or the *von Karman turbulence model* [17], which expresses the distribution of energy of small scale turbulent motions. Standard reconstruction algorithms use the related atmospheric phase covariance matrix C_Φ as regularization operator by enforcing $\|C_\Phi^{-1/2}\Phi\|$ to be bounded. Following [4], we have for the Kolmogorov model

$$\|C_\Phi^{-1/2}\Phi\|^2 \propto \int |\widehat{\Phi}(\omega)|^2 |\omega|^{11/3}\, d\omega \;,$$

which suggests $\Phi \in H^{11/6}$.

Thus, the atmospheric model leads us to expect a much higher smoothness for the functions representing turbulences than just L^2, which is the reason for choosing $V_\ell = H^1(\Omega_l)$ in the H^1-case. As we will see in Section 3.4, the use of the adjoint H^1 embedding operator will lead to atmospheric layers with the expected smoothness.

3.2 Algorithmic Description of the Smoothed Landweber-Kaczmarz Iteration

Noting that $\mathrm{i}_\ell^* : L^2(\Omega_\ell) \to H^1(\Omega_\ell)$ is given by the relation

$$\langle \mathrm{i}_\ell w,\, v\rangle_{L^2(\Omega_\ell)} \;=\; \langle w,\, \mathrm{i}_\ell^* v\rangle_{H^1(\Omega_\ell)} \qquad \text{for } w \in H^1(\Omega_\ell),\ v \in L^2(\Omega_\ell),$$

it follows immediately that $u = \mathrm{i}_\ell^* v \in H^1(\Omega_\ell)$ is the solution of the variational problem

$$\int_{\Omega_\ell} \sigma \nabla u \cdot \nabla w + u\, w\, dx \;=\; \int_{\Omega_\ell} v\, w\, dx \qquad \forall w \in H^1(\Omega_\ell), \tag{11}$$

where σ is the positive parameter from (8). This is in turn the variational formulation of the *classical* Neumann boundary value problem

$$\begin{aligned} u - \sigma \Delta u \;&=\; v \qquad && \text{in } \Omega_\ell \\ \frac{\partial u}{\partial \boldsymbol{n}} \;&=\; 0 \qquad && \text{on } \partial\Omega_\ell\,, \end{aligned} \tag{12}$$

where $\boldsymbol{n}$ is the outward unit normal to $\partial\Omega_\ell$ (cf., e.g., [6, 13] and also [16]).

Apparently, in order to apply the adjoint operator $\mathbf{i}^* = (\mathrm{i}_1^*, \ldots, \mathrm{i}_L^*)$ in the H^1-case, we have to solve an elliptic partial differential equation on each of the domains Ω_ℓ of overlapping telescope apertures. Although the solution u of (11) is a priori sought in $H^1(\Omega_\ell)$, one can prove higher *regularity*. In Section 3.4, we will show that $u \in H^s(\Omega_\ell)$ for some $s \in (3/2, 2]$. The solution u of (11) can be seen as a *smoothed* version of the corresponding "source function" v. The parameter $\sigma > 0$ controls the strength of the smoothing, and we discuss its choice further in Section 3.3.

Thus, we end up with Algorithm 1, a Landweber-Kaczmarz iteration with an additional smoothing step based on solving (12) (cf. [16, 5]). Note that the smoothing can be done independently on each layer, and may, thus, be straightforward *parallelized*.

Algorithm 1 Smoothed Landweber-Kaczmarz iteration.

Require: $\varphi_g,\ g = 1, \ldots, G$ # Incoming wavefronts
Require: $\Phi^{(0)}$ # Initial guess
  $i \leftarrow 1$
  repeat
    for $g = 1, \ldots, G$ **do** # Loop over all guide stars
      $r \leftarrow \varphi_g - \boldsymbol{A}_g \Phi^{(i-1)}$ # Evaluation of residual
      $a \leftarrow \boldsymbol{A}_g^*\, r$ # Application of L^2 adjoint operator (7)
      $s \leftarrow \mathbf{i}^*\, a$ # Smoothing via (11)
      $\Phi^{(i)} \leftarrow \Phi^{(i-1)} + \beta_i\, s$ # Weighted update
      $i \leftarrow i + 1$
    end for
  until stopping criterion fulfilled

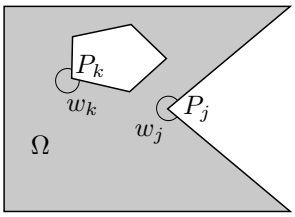

Figure 2: A polygonal domain with corner points P_j and interior angles ω_j.

3.3 Choice of the Parameter σ

The fact that the parameter $\sigma > 0$ controls the strength of the smoothing operation $\mathbf{i}_\ell^*$ (see (11)) is seen from the following extreme cases: $\sigma = 0$ corresponds to the L^2-case, i.e., $u = v$ and no smoothing occurs. For $\sigma \to \infty$, the solution u tends to a constant.

To get a real smoothing effect without too much blur, the parameter σ has to be chosen carefully, typically small. Note that, because σ occurs in front of the Laplace operator, it should be chosen proportional to the square of the length scale of the problem. In our application, we do not compute $\mathbf{i}_\ell^*$ exactly, but solve a discretized version of (11) with finite differences. Therefore, σ should be adapted to the mesh size. In our computations we use the (experimentally tuned) choice $\sigma \approx h^2$, where h is the mesh size.

3.4 Analysis of the Smoothing Operations $\mathbf{i}_\ell^*$

In this section, we investigate the smoothness of the layers after the application of the H^1-adjoint, i.e., we will provide an estimate for $s \in (3/2, 2]$ such that the solution u of (11) fulfills $u \in H^s(\Omega_\ell)$.

The regularity of solutions of elliptic PDEs has been studied intensively (cf., e.g., [2, 9, 10]). In general, it depends on the shape of the computational domain, on the boundary conditions, and on the data.

Since in practice all data gathered by wavefront sensors are provided on a regular finite grid, the set Ω_T is never an exact annullus but rather an approximation of it, where the boundaries are polygons. Therefore, we may restrict our analysis to polygonal domains Ω, i.e., Ω is a connected bounded open subset of $\mathbb{R}^2$, where the outer boundary and the inner boundaries (if holes exist) are polygons. The corner points and corresponding interior angles are denoted by P_i and ω_i, respectively, $i = 1, \dots, n$ (see Figure 2).

Our smoothness result is based on the following theorem for polygonal domains:

Theorem 3.1. *Let Ω be a polygonal domain and let $f \in L^2(\Omega)$ be such that $\int_\Omega f\,dx = 0$. Then there exists a solution $u \in H^1(\Omega)$ (unique up to a constant) of the problem*

$$\int_\Omega \nabla u \cdot \nabla w\,dx = -\int_\Omega f\,w\,dx \qquad \forall w \in H^1(\Omega)\,.$$

Moreover, there exist functions S_i and unique numbers c_i such that

$$u - \sum_{\substack{i=1\\ \omega_i > \pi}}^{n} c_i S_i \in H^2(\Omega)\,.$$

The functions S_i have local support around the corners P_i and have the property that $S_i \in H^s(\Omega)$ for all $s < \pi/\omega_i$. Thus, $u \in H^s(\Omega)$ for all $s \le 2$ with

$$s < 1 + \frac{\pi}{\max\limits_{i\in\{1,\dots,n\}} \omega_i}.$$

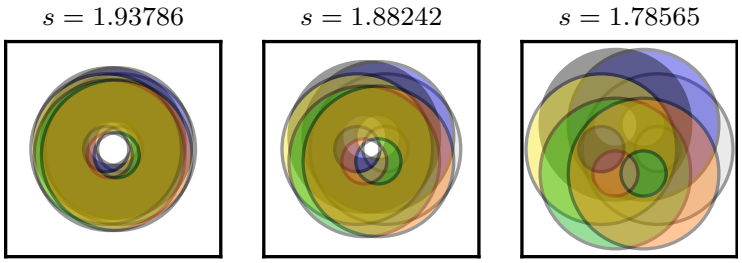

Figure 3: Expected regularity $u \in H^s(\Omega_\ell)$ in a nine layer model. Only the highest three layers located at 4500m, 9000m, 18000m are shown (left to right).

Proof. The proof follows immediately with [9, Theorem 4.4.4.13] and [10, Theorem 1.2.18 and Corollary 2.4.4]. □

According to this theorem the regularity of the solutions u depends on the degree of non-convexity of the polygonal domain, or more precisely, on the largest non-convex interior angle ω_i. For a convex polygonal domain we get $u \in H^2(\Omega)$. On non-convex polygonal domains however, the solutions u contain singular components, which results in the reduced regularity $u \in H^s(\Omega)$ for some $s \in (3/2, 2)$.

Corollary 3.2. *Let Ω_ℓ be a polygonal domain, let $v \in L^2(\Omega_\ell)$, and let $\sigma > 0$. Then problem (11) has a unique solution $u \in H^1(\Omega)$. Moreover, $u \in H^s(\Omega)$ for all $s \leq 2$ with*

$$s < 1 + \frac{\pi}{\max\limits_{i \in \{1,\dots,n\}} \omega_i}.$$

Proof. The existence and uniqueness of $u \in H^1(\Omega)$ follow from the Lax-Milgram Lemma (cf., e.g., [1]). Noting that u then also solves the problem

$$\int_{\Omega_\ell} \nabla u \cdot \nabla w \, dx = -\int_{\Omega_\ell} f \, w \, dx \qquad \forall w \in H^1(\Omega_\ell)$$

for $f = \sigma^{-1}(u - v)$, the regularity result immediately follows from Theorem 3.1. □

Recall that the particular domains Ω_ℓ consist of overlapping shifted telescope apertures. Assuming that the annular region Ω_T is approximated sufficiently fine by polygons such that only the angles at intersection points determine the regularity, it is clear that, in case of an increased field of view or higher up in the atmosphere, the interior angles increase. Consequently, this leads in turn to a decrease in the regularity of solutions of (11). Figure 3 shows the expected regularity according to Corollary 3.2 for some atmospheric layers. One can see how with increasing layer altitudes, the telescope apertures separate further and further, enlarge the non-convex angles, and thereby reduce the (expected) regularity.

In some cases, especially when using Shack-Hartman wavefront sensors, Ω_T is usually a collection of quadratic subapertures. Thus, all interior non-convex angles in Ω_ℓ are equal to $3\pi/2$. According to Corollary 3.2 the expected regularity of the solutions will then be $s < 1 + 2/3$.

4 Numerical Results

To test the the smoothed Landweber-Kaczmarz method that was derived in Section 3, this functionality was implemented in an MCAO simulation framework developed by the *Mathematical algorithms and software for ELT adaptive optics* project, a joint work by the *Institute*

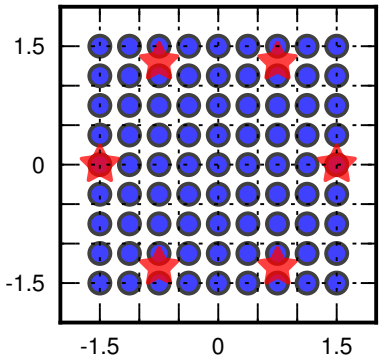

Figure 4: Angular positions of guidestars (red stars) and evaluation directions (blue circles) (units are in arc minutes).

for Industrial Mathematics at the *Johannes Kepler University*, the *Johann Radon Institute for Computational and Applied Mathematics* (RICAM) and the *Industrial Mathematics Competence Center* (IMCC). The tests were performed in a realistic setting using data from the *European Southern Observatory* (ESO) and designs for the *European Extremely Large Telescope* (E-ELT).

Von Karman turbulence was used to model turbulent layers in the atmosphere. There are different ways to generate random turbulences following this statistical model. One popular method is to use the equation for the Von Karman turbulence directly using a Fourier transform approach. The periodicity that is caused by using the Fourier transform is particularly useful when shifting the layers to simulate winds for closed-loop operation. See for example [12, 21] for more information on simulating atmospheric turbulence. To simulate a full atmosphere, a model consisting of *nine independent layers* was used, with realistic values for heights and turbulence strengths provided by the ESO.

The tests used parameters corresponding to E-ELT designs. Six Shack-Hartmann wavefront sensors with a resolution of 84x84 pixels were used to observe natural guide stars arranged in a circle (see Figure 4 about the geometry). Three deformable mirrors were conjugated at ground level, 4km, and 12km altitude, respectively.

The Shack-Hartmann wavefront sensors provide data on regular grids, so a finite difference method was used to model the partial differential equation (12). The resolution of the discretization of the domains Ω_ℓ was chosen to match the wavefront sensor resolution. Whereas at lower atmospheric layers, large areas of the different wavefront sensors overlap (see Figure 3), at higher layers these areas are spread out more, leading to slightly bigger systems for solving (12) on those layers. The use of higher resolutions and more sophisticated meshing strategies are not investigated in the present paper.

As possible solvers for the resulting sparse systems of linear equations, both PCG and direct methods based on sparse LU-factorization were considered. For the problem sizes at hand, both methods performed well. PCG was tested with incomplete LU preconditioning and typically required only two iterations to converge to a sufficiently good solution. For the highest atmospheric layer in the nine layers model used in the tests, the system matrix consists of about 52,000 nonzero entries. The sparse LU factorization of this matrix results in a system with about 2 million nonzero entries. The CG method with incomplete LU factorization as a preconditioner (using Matlab's `ilu` function with the parameter `drop tolerance` set to 10^{-5}) requires storing about 325,000 nonzero elements. Smoothing all layers on a 2.5 GHz processor took about 0.02 seconds with the direct method and 0.05 seconds using PCG. However, layers are smoothed independently of each other, so these computations can be executed in parallel.

For the smoothed Landweber-Kaczmarz iteration, we used the parameter choice $\sigma = 0.2 \approx$

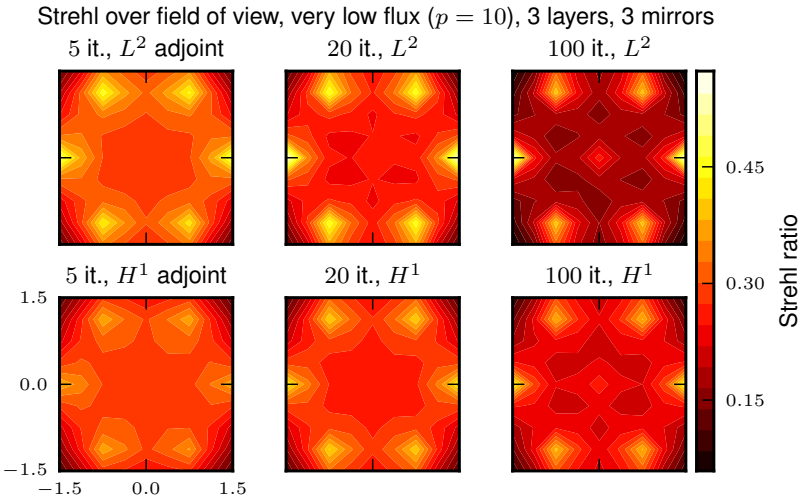

Figure 5: Strehl ratios on field of view for different iterations with and without additional smoothing.

$(40/84)^2$, here depending on the diameter of $40m$ of the telescope and the number 84 of grid points in each direction, cf. Section 3.3.

To evaluate the performance of the smoothed Kaczmarz-Landweber method, we used the *Strehl* ratio, which measures how strongly light from a single source is spread out, compared with the best possible focus (as dictated by the diffraction limit). The maximum value is 1.0 and a lower value indicates a decrease in image resolution due to optical imperfections in the telescope optics and image distortions due to atmospheric turbulences. To calculate the Strehl ratio, we have used the Maréchal approximation (cf., e.g., [19]) $S \approx e^{-\bar{\sigma}^2}$, where $\bar{\sigma}^2$ denotes the variance in the residual phase (after correction by the deformable mirrors). This measure was evaluated for a number of directions in the sky, as shown in Figure 4.

4.1 Tests

4.1.1 Fixed Photon Flux

In Figure 5, we have plotted a contour map of the Strehl ratio for the entire field of view (3 arcminutes) for the original L^2-case reconstructors and the corresponding H^1-case reconstructors for different iteration numbers. Note that the hot spots at 1.5 arcminutes distance from the centre correspond to the direction of the guide stars (Figure 4). Generally, we see how the reconstruction focuses more and more on the guidestar directions, as we iterate. The smoothing (second row) helps "spread out" the correction from those spots towards the centre of the field of view. Figure 6 shows the Strehl ratios as a function of the distance from the centre of the field of view, where we can see more clearly, what effect the smoothing has on the reconstruction. In these cases, the solvers were tasked with reconstructing a *three layers atmosphere* (as compared to the actual nine layers atmospheric make-up). This corresponds to cases with insufficient available a-priori knowledge of the actual atmospheric structure, or to cases where computational concerns lead to the decision to reconstruct only an approximate atmosphere.

In Figures 7 and 8 we see the corresponding tests, where the reconstructors where provided an accurate atmospheric model as a-priori information. One immediately sees, how much the Strehl ratios have improved compared to the previous test.

With regards to the smoothing, we can observe two different effects. In the three reconstructed layers case, the smoothing is able to increase the Strehl ratio particularly in the inner

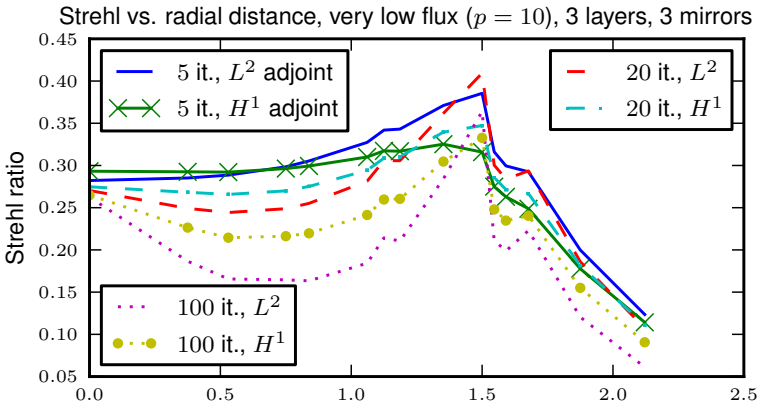

Figure 6: Strehl ratios on field of view for different iterations with and without additional smoothing.

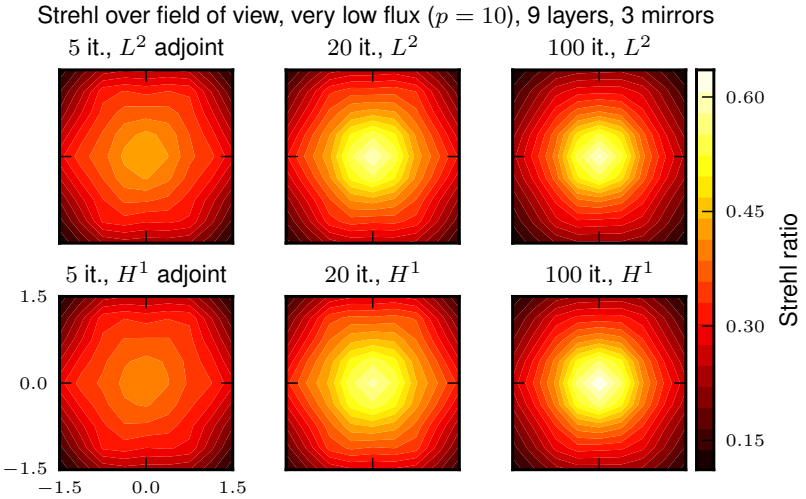

Figure 7: Strehl ratios on field of view for different solutions.

field of view, where the astronomical object under observation is located. In the nine layers reconstruction the smoothing spreads the correction factor outwards from the centre, which might be useful when observing wide-spread astronomical targets.

We also see that the three layers case is so badly conditioned, that additional iterations past the first few actually degrade the quality of the solution; an effect that is not present in the better conditioned nine layers case.

4.2 Noisy Layer Altitudes

To simulate uncertainty in a-priori knowledge of the atmospheric structure, we have taken the nine layer atmosphere and slightly modified each layer's altitude by up to ±5%, so that the reconstructed layers, i.e. the a-priori model, doesn't match the actual structure exactly anymore.

The results for a nine layers reconstruction can be seen in Figure 9. Comparing with the previous section's results, it is clear just how important a-priori information is. Not surprisingly, the results are much worse than in the case of completely accurate a-priori information, but still better than in the very inaccurate case of trying to reconstruct only three layers. The

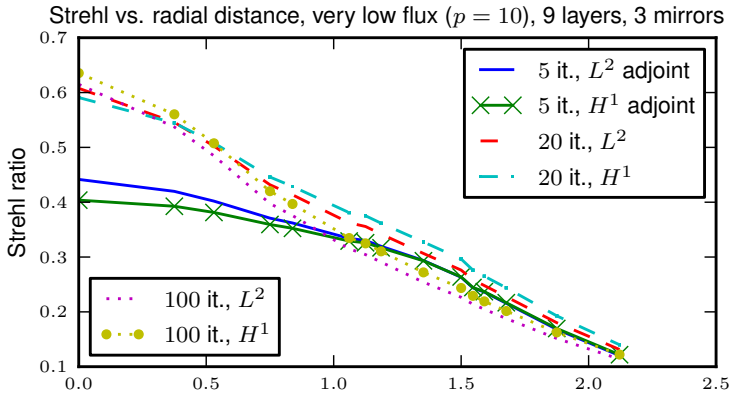

Figure 8: Strehl ratios vs. radial distance.

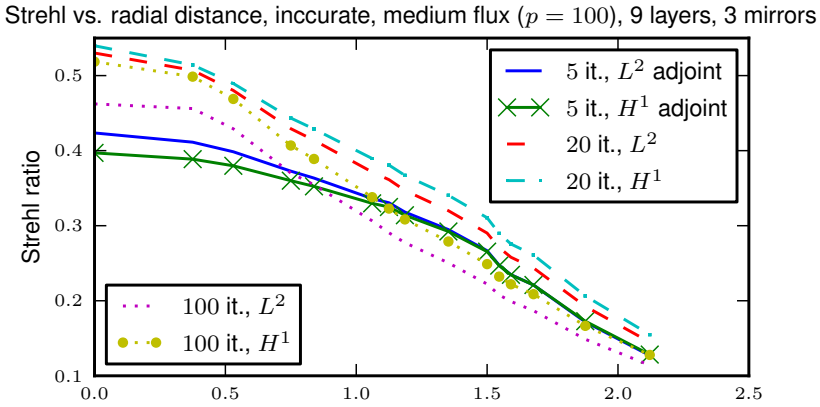

Figure 9: Strehl ratios on field of view for different iterations with and without additional smoothing. The altitudes of the reconstructed layers do not precisely match the actual atmospheric layer heights, but randomly perturbed by about ±10%.

additional smoothing step is capable of maintaining a much higher Strehl ratio in the face of such imprecisions. Also note that now the problem is conditioned badly enough for the 100 iterations case to be worse than the 20 iterations case.

4.2.1 Different Photon Flux Levels

Next, we will investigate the effect that the photon flux level has on the performance of various reconstruction methods.

Starting with a three layers reconstruction, in Figure 10 we have plotted the average Strehl ratio of several reconstructors for different photon flux levels. The average was taken on the inner field of view with a diameter of approximately 0.5 arcminutes. We can see that the smoothing improves the reconstruction results in the inner field of view for all photon flux levels. Even so, in this very badly conditioned test case, fewer iterations are still better than high iteration numbers. (However, there are many more potential sources of noise in an adaptive optics system, which might offer more potential for the application of the smoothed Kaczmarz-Landweber method.)

Next, Figure 11 shows the same analysis but with nine reconstructed layers. Again we notice how, due to more precise a-priori information, we can now achieve higher iteration numbers before the reconstruction quality degrades. We see that for few iterations, the smoothing is actually harmful to the reconstruction effort, however, as the iteration numbers increase,

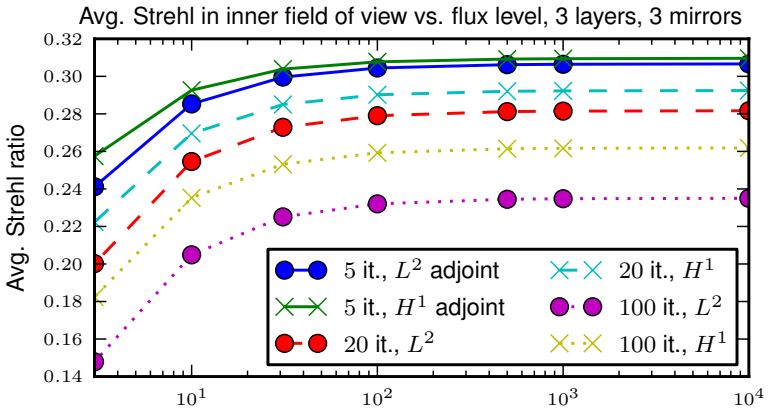

Figure 10: Average Strehl ratio in inner field of view for different photon flux levels.

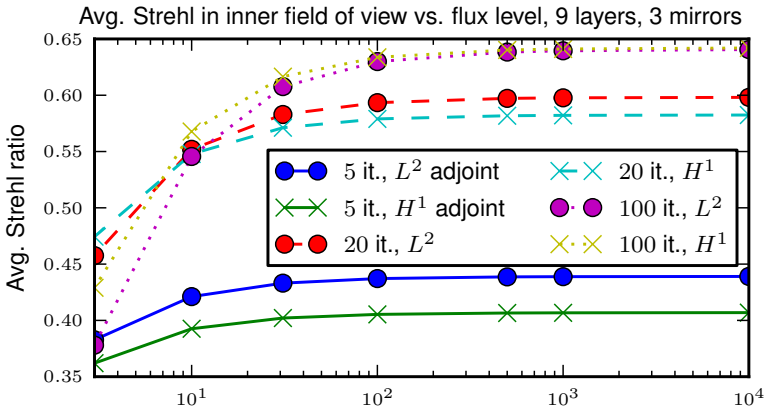

Figure 11: Average Strehl ratio in inner field of view for different photon flux levels.

the smoothing becomes more and more effective. Note in particular, how the 100 iterations solutions are the best solutions for photon fluxes $p > 10$, whereas below that limit the 20 iterations solution performs better.

References

[1] S. C. Brenner and L. R. Scott. *The Mathematical Theory of Finite Element Methods*, volume 15 of *Texts in Applied Mathematics*. Springer, New York, second edition, 2002.

[2] M. Dauge. *Elliptic boundary value problems on corner domains: smoothness and asymptotics of solutions*. Lecture notes in mathematics. Springer-Verlag, 1988.

[3] P. P. B. Eggermont, G. T. Herman, and A. Lent. Iterative algorithms for large partitioned linear systems, with applications to image reconstruction. *Linear Algebra and its Applications*, 40:37 – 67, 1981.

[4] B. Ellerbroek. Efficient computation of minimum-variance wave-front reconstructors with sparse matrix techniques. *J. Opt. Soc. Am.*, 19(9):1803–1816, 2002.

[5] M. Eslitzbichler. A Sobolev space smoother for atmospheric tomography in multi conjugate adaptive optics. Master's thesis, Johannes Kepler Universität Linz, 2012.

[6] L. Evans. *Partial Differential Equations*. Graduate Studies in Mathematics. American Mathematical Society, 1998.

[7] L. Gilles and B. L. Ellerbroek. Split atmospheric tomography using laser and natural guide stars. *J. Opt. Soc. Am. A*, 25(10):2427–2435, Oct 2008.

[8] L. Gilles, B. L. Ellerbroek, and V. C. R. A comparison of multigrid V-cycle versus Fourier domain preconditioning for laser guide star atmospheric tomography. In *Adaptive Optics: Analysis and Methods/Computational Optical Sensing and Imaging/Information Photonics/Signal Recovery and Synthesis Topical Meetings on CD-ROM*. Optical Society of America, 2007. `http://www.opticsinfobase.org/abstract.cfm?URI=AO-2007-JTuA1`.

[9] P. Grisvard. *Elliptic problems in nonsmooth domains*. Monographs and studies in mathematics. Pitman Advanced Pub. Program, 1985.

[10] P. Grisvard. *Singularities in boundary value problems*. Recherches en mathématiques appliquées. Masson, 1992.

[11] S. Kaczmarz. Angenäherte Auflösung von Systemen linearer Gleichungen. *Bulletin International de l'Académie Polonaise des Sciences et des Lettres*, 35:355–357, 1937.

[12] R. Lane, A. Glindemann, and J. Dainty. Simulation of a Kolmogorov phase screen. *Waves in Random Media*, 2(3):209–224, 1992.

[13] W. C. H. McLean. *Strongly elliptic systems and boundary integral equations*. Cambridge University Press, 2000.

[14] F. Natterer. *The Mathematics of Computerized Tomography*. Classics in Applied Mathematics. Society for Industrial and Applied Mathematics, 2001.

[15] R. Ragazzoni, E. Marchetti, and F. Rigaut. Modal tomography for adaptive optics. *Astronomy and Astrophysics*, 342:L53–L56, 1999.

[16] R. Ramlau and M. Rosensteiner. A Kaczmarz type reconstructor for MCAO data. Technical report, 2011. submitted for publication.

[17] F. Roddier. The effects of atmospheric turbulence in optical astronomy. *Progress in optics. Volume 19. Amsterdam, North-Holland Publishing Co., 1981, p. 281-376.*, 19:281–376, 1981.

[18] M. Rosensteiner. Wavefront reconstruction for extremely large telescopes via CuRe with domain decomposition. *J. Opt. Soc. Am. A*, 29(11):2328–2336, Nov 2012.

[19] T. S. Ross. Limitations and applicability of the Maréchal approximation. *Appl. Opt.*, 48(10):1812–1818, Apr 2009.

[20] M. Tallon and R. Foy. Adaptive telescope with laser probe - Isoplanatism and cone effect. *Astronomy and Astrophysics*, 235:549–557, 1990.

[21] A. M. Vorontsov, P. V. Paramonov, M. T. Valley, and M. A. Vorontsov. Generation of infinitely long phase screens for modeling of optical wave propagation in atmospheric turbulence. *Waves In Random And Complex Media*, 18(1):91–108, 2008.

[22] Q. Yang, V. C. R., and B. L. Ellerbroek. Fourier domain preconditioned conjugate gradient algorithm for atmospheric tomography. *Appl. Opt.*, 45(21):5281–5293, 2006.

[23] M. Zhariy, A. Neubauer, M. Rosensteiner, and R. Ramlau. Cumulative wavefront reconstructor for the Shack-Hartmann sensor. *Inverse Problems and Imaging*, 5(4):893–913, 2011.

Latest Reports in this series

2009 - 2010

[..]

2011

[..]

2011-09	Michael Kolmbauer *Efficient Solvers for Multiharmonic Eddy Current Optimal Control Problems with Various Constraints*	November 2011
2011-10	Markus Kollmann, Michael Kolmbauer, Ulrich Langer, Monika Wolfmayr and Walter Zulehner *A Finite Element Solver for a Multiharmonic Parabolic Optimal Control Problem*	December 2011

2012

2012-01	Markus Kollmann and Walter Zulehner *A Robust Preconditioner for Distributed Optimal Control for Stokes Flow with Control Constraints*	January 2012
2012-02	Michael Kolmbauer and Ulrich Langer *A Robust Preconditioned MinRes-Solver for Time-Periodic Eddy Current Problems*	January 2012
2012-03	Wolfgang Krendl, Valeria Simoncini and Walter Zulehner *Stability Estimates and Structural Spectral Properties of Saddle Point Problems*	February 2012
2012-04	Helmut Gfrerer *On Directional Metric Regularity, Subregularity and Optimality Conditions for Nonsmooth Mathematical Programs*	February 2012
2012-05	Veronika Pillwein and Stefan Takacs *A Multigrid Fourier Analysis of a Multigrid Method using Symbolic Computation*	April 2012
2012-06	Stefan Takacs and Walter Zulehner *Convergence Analysis of All-at-once Multigrid Methods for Elliptic Control Problems Under Partial Elliptic Regularity*	June 2012
2012-07	Helmut Gfrerer *On Directional Metric Subregularity and Second-Order Optimality Conditions for a Class of Nonsmooth Mathematical Programs*	August 2012
2012-08	Michael Kolmbauer and Ulrich Langer *Efficient Solvers for Some Classes of Time-Periodic Eddy Current Optimal Control Problems*	November 2012
2012-09	Clemens Hofreither, Ulrich Langer and Clemens Pechstein *FETI Solvers for Non-Standard Finite Element Equations Based on Boundary Integral Operators*	November 2012
2012-10	Helmut Gfrerer *On Metric Pseudo-(sub)Regularity of Multifunctions and Optimality Conditions for Degenerated Mathematical Programs*	December 2012
2012-11	Clemens Pechstein and Clemens Hofreither *A Rigorous Error Analysis of Coupled FEM-BEM Problems with Arbitrary Many Subdomains*	December 2012
2012-12	Markus Eslitzbichler, Clemens Pechstein and Ronny Ramlau *An H^1-Kaczmarz Reconstructor for Atmospheric Tomography*	December 2012

From 1998 to 2008 reports were published by SFB013. Please see
`http://www.sfb013.uni-linz.ac.at/index.php?id=reports`
From 2004 on reports were also published by RICAM. Please see
`http://www.ricam.oeaw.ac.at/publications/list/`
For a complete list of NuMa reports see
`http://www.numa.uni-linz.ac.at/Publications/List/`